www.vbripress.com/aml, DOI: 10.5185/amlett.2016.6036

Synthesis and characterization of ring shaped spermine mediated nanogold assemblies at the air water interface

Divya Sachdev[1], Shweta Gupta[3,2], Veeresh Kumar[3] , Sandeep Singh[3] and Renu Pasricha[4*]

[1]*National Institute of Food Technology, Entrepreneurship and Management, Sonipat, India*
[2]*Department of Chemistry, University of Delhi, Delhi 110007, India*
[3]*National Physical Laboratory, CSIR, Dr. K.S. Krishnan Road, New Delhi 110012, India*
[4]*National Centre for Biological Sciences, TIFR, Bangalore 560065, India*

[*]Corresponding author. E-mail: renu1505@gmail.com

Received: 25 June 2015, Revised: 10 October 2015 and Accepted: 05 March 2016

ABSTRACT

Surface tension mediated U-shaped interlinked diammine network (spermine) assembled at the air-water interface, when interacted with aqueous functionalized gold nanoparticles (AuNPs), form ring like nanogold structures. These electrostatic force guided self-assembies of the ligand diammine with gold provides a facile route for control on the nanostructure formation while portraying double linkage ability of the diammine (here spermine). Pressure-area isotherm of controlled multilayer formation of spermine linked gold NPs (spermine-AuNPs) were studied and characterized by UV-Vis spectroscopy, Fourier transform infrared spectroscopy and Transmission electron microscopy (TEM). The TEM micrographs clearly elucidate the formation of ring like networks of gold NPs under the influence of spermine. Furthermore we believe that these spermine-AuNPs will surely have supportive role as a bio-diagnostic material for ultra-sensitive biological detection and pave way for a novel route for assembly fabrication. Copyright © 2016 VBRI Press.

Keywords: Air-water interface; interlinked networks; gold nanoparticle; pressure-area isotherm; spermine.

Introduction

Patterning gold and silver nanoparticles using biomolecular matrix for generating 2D self-assemblies or new configurations have a unique role and may lead to applications in optic, electronic and photonic materials desired for bio-diagnostics [**1-3**]. Although different approaches have been explored for the synthesis of thin films especially self-assembly of the nanoparticles in 2-D structures; such as solvent evaporation [**4**], immobilization by covalent attachment at the surfaces of self-assembled monolayers [**5-6**] use of surface modified polymers [**7**], electrophoretic assembly [**8**], DNA-mediated assembly in thin film form [**9-10**] or diffusion into ionizable fatty lipid films [**11**] but synthesis of organized arrays of bioinorganic assemblies depicting biological structure-function relationships are very few .Since organization of these molecular systems into functional structures and actuation of these assemblies in living systems will be significant and hence methods are devised for encapsulation of drug for therapeutic purposes wherein biogenic nanostructures behave as a receptor and are fairly recognized within the biological environment [**12-13**].

Biomolecules like DNA, proteins and viruses have shown their capability as a templating agent for 2-D nano-assemblies [**14**]. Incorporating these biomolecules inside the nanoparticles facilitates and creates versatility in the intrinsic properties of the nano-assemblies. C. KIM [**12**] have revealed the application of enhanced drug delivery of such bio-nanomolecular systems (host-guest) featuring platinum based drugs encapsulated inside the cavity of diaminohexane-terminated gold NPs (AuNPs-NH_2) and complementary curcurbit(7) uril [**15**]. The host-guest property in a material facilitates the release of therapeutic power of the drug triggered via competitive complexation. Recently organized nanostructures via polycomplexation of dispersed nanoparticles like (Fe, Au, Pd) to polyamines, DNA were also synthesized by different routes by Khomutov [**16-18**] for biomedical applications [**2,19-20**].

Past Decade has shown considerable interest in the synthesis of ordered arrays of gold NPs using Langmuir-Blodgett (LB) method, which allows a precise control on organization of surfactant-stabilized nanoparticles at air–water interface [**21-26**].Very few groups have used the interface as dynamic platform for the synthesis and functionalization of multilayered colloidal films of gold NPs by controlling the electrostatic interaction [**27-30**]. Although the monofunctional amphiphilic molecules have been widely investigated with respect to their behavior for the mere assembly or in dynamic mode at the LB surface with gold NPs but there are no reports on forming the structured assembly of gold NPs using bolafoms amphiphilic molecules wherein Langmuir-Blodgett (LB) surface contribute as an active medium for bringing the two reactive moieties in close proximity.

Bolafom amphiphilic molecules are composed of hydrophobic skeleton with two hydrophilic sites which are fairly separated by some distance, despite their physiological characteristics such as solubility in water and self-assembling property these molecules have not received much attention [**31**]. Even though bolafoms adsorb at the air-water interface but are much less efficient than the corresponding conventional surfactants in lowering the surface tension of water [**32**]. The values of the surface area per surfactant suggest that most bolaforms adopt a wicket-like or looped conformation at the air-water interface, with the polar groups anchored at the interface and the alkyl chain forming more or less wide loop in the air [**33-34**] whereas few bolafoms have been reported to lie flat at the interface [**35**]. The formations of such structures have been theoretically reported [**36-37**]. Recent investigations by Paczesny[38]have also shown the formation of ordered 2D arrays of covalently linked bolampiphile gold NPs via drop-casting method.

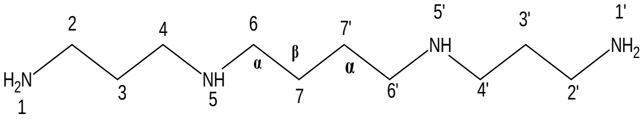

Fig. 1. Structure of the spermine molecule.

Herewith, we report the linking of diaminopropyltetramethylenediamine (spermine, **Fig. 1**) with gold NPs through electrostatic binding at the air water interface and we propose that spermine forms a U-shaped structure at the air-water interface on interaction with gold NPs resulting in ring-like morphologies. This technique needs high precision and control which is evident from the fact that films consisting of bolofom and gold nanoparticles conjugated structures could not be fabricated by Paczesny [**38**] and group and they switched to drop casting method. It is difficult to mimic the exact conditions of the air water interface using drop casting technique so there is no comparision in the structures of the nanoparticles achieved in this report and by drop casting. Although an experiment was also conducted by us to predict the geometry of the drop casted Au-NPs stabilized by ligand citrate (supplementary information, **Fig. S3**), to investigate the ring formations of AuNPs, but very few circular arrangements were observed corroborating our purpose to use spermine. We envisage that this cross-linked structure of spermine with gold will have a promising future as photoprobes [**2,19-20**] and biosensing applications.

Experimental

Synthesis of gold NPs (Au NPs)

All chemicals were purchased from Sigma-Aldrich and were used as received without further purification. All solutions were prepared using Millipore (resistivity-18.2 MΩ/cm) water. Gold NPs were synthesized as described in the literature [**29**]. In a typical experiment 0.01g of sodium borohydride ($NaBH_4$) was dissolved in 10 ml (Millipore water) and was transferred drop-wise to 100ml of 10^{-4} M hydroaurochloric acid ($HAuCl_4$) aqueous solution. In order to prevent aggregation of gold NPs the reducing agent was added drop wise at room temp (30°C) and pH 9. The gold solution in flask changed to ruby-red color indicating the formation of gold nanoparticles(AuNPs) [**39**].

For the synthesis of interlinked assemblies of gold NPs using diamine as linker, stock solution of 1mg/mL spermine (**Fig.1**) in chloroform was prepared and spread over the Au colloid subphase at pH = 4.5using a micro-syringe in a drop wise manner till the formation of lens on subphase.

After allowing a waiting period of 30 min for solvent evaporation, the monolayer was compressed at a constant rate of 10 mm/min. Surface pressure-area isotherm was recorded after 30 min, 2 h and 3 h, respectively with Wilhelm plate as the surface-pressure sensor for the LB trough.

Characterization of LB-films

The absorption spectrum was recorded using a UV 1800 Shimadzu spectrophotometer. Tecnai G^2 F30 S-Twin (FEI; Super Twin lens with Cs =1.2 mm) instrument operating at an accelerating voltage of 300 kV having a point resolution of 0.2 nm and lattice resolution of 0.14 nm with attached energy-dispersive X-ray spectrometer (EDS) was used for high resolution transmission electron microscopy (HRTEM). Program Digital Micrograph (Gatan) was used for image processing. Apex LB trough, Model 220 was used for the all Pressure-Area studies. Fourier transform Infrared (FTIR) spectroscopy was performed using Nicolet 5700 FTIR spectrometer. Contact angle measurements were performed using drop shape analogy system Model DSA-10 MK2 (KrussGmbh).Tapping mode AFM images were recorded using Multimode-V, Veeco Instruments.

Transfer of LB films for characterization

Films of the spermine as well as spermine-AuNPs of different thickness were formed by the versatile LB technique at a surface pressure of 30mN/m and a deposition rate of 15 mm/min with a waiting time of 1min between dips, in case of deposition of multilayers. LB films were deposited on quartz slides, Si (111) wafers, and carbon-coated transmission electron microscopy (TEM) grids for UV-Vis spectroscopy, Fourier transform infrared spectroscopy (FTIR), and electron microscopy measurements respectively. Three mono-layers of lead arachidate were deposited on the quartz and Si (111) substrates to make them hydrophobic before transferring the mono-layers. The hydrophobization of the substrate ensures better transfer ratios of then on particle mono-layers. Contact angle measurements were carried out on the multilayer films deposited on quartz substrates.

Results and discussion

In order to explain the formation of assembly of gold NPs in presence of spermine, initial behavior of spermine molecules at air-water interface was analyzed. When surfactant concentration is less than critical micellar concentration (CMC), the surfactant molecules execute a random motion on the water–air interface. This tendency can be explained by surface-energy considerations, since the tails are hydrophobic, their exposure to air is favored instead on water. However the heads are hydrophilic, the head–water interaction is more favorable than air–water interaction. The overall effect is reduction in the surface energy (or equivalently, surface tension of water).The formation of monolayer at the air water interface is thus is dependent on the CMC (critical micellar concentration) which was experimentally found to be 10^{-3} M (Supporting information **Fig. S1, S2**). Surface pressure-area isotherm (π-A) measurements are the conventional way to characterize the phase behavior of Langmuir monolayers.

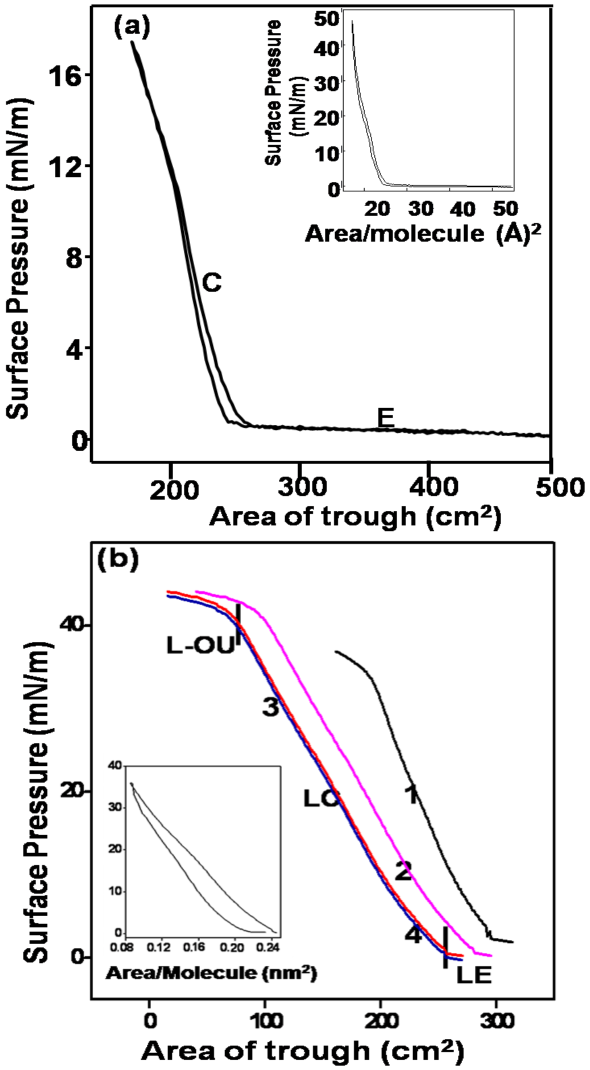

Fig. 2. π-A Isotherm of (a) ODA on water as subphase. (b) Spermine on water as subphase. Curve 1; after 30 min of spreading of spermine; Curve 2; after 2 h of spreading of spermine; Curve 3.after 3 h on addition of spermine. (Inset of (a) and (b) shows area of the molecule Vs surface pressure for ODA and spermine respectively).

Fig. 2 (b) shows the π-A isotherm of the spermine monolayer on aqueous subphase at different time intervals. Measurements were obtained during both the compression and expansion cycles of spermine monolayer at the interface. It was observed that during compression the surface pressure builds up to reach the limiting value of 39mN/m and further compression leads to collapse of monolayer.

The increase of surface pressure indicates an inherently large flexibility of the long carbon chain. **Fig. 2 (b)**, Curve1 indicates the decrease in surface area from 293 to 192 cm^2 with increase in pressure.

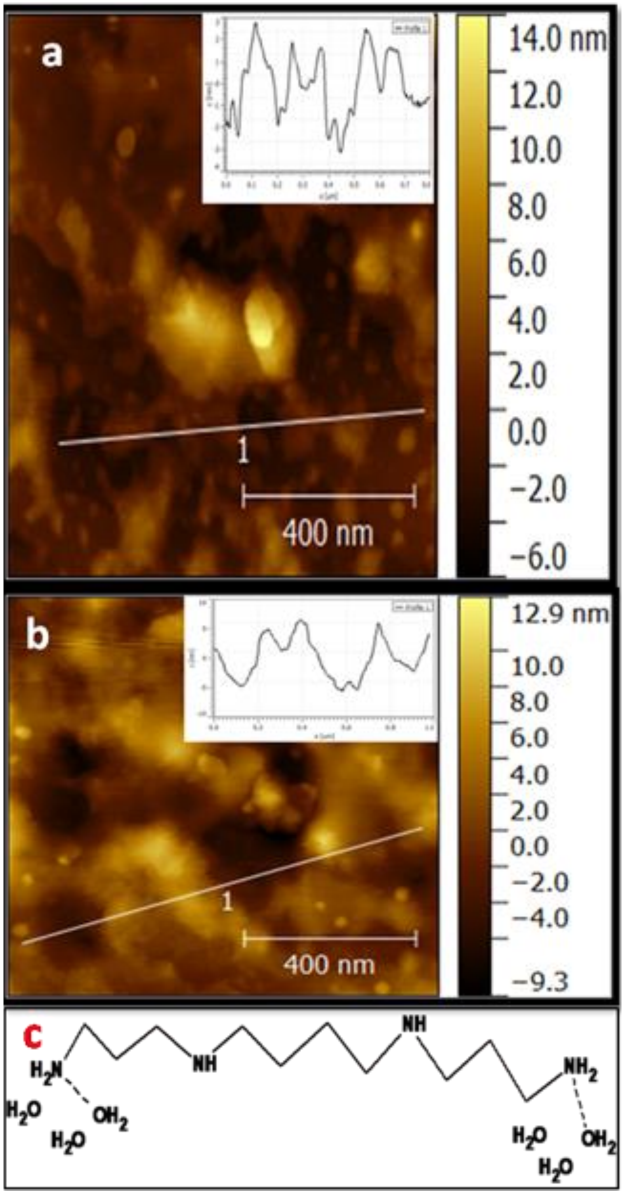

Fig. 3. AFM images of spermine monolayer on silicon wafer transferred (a) at surface pressure of 3mN/m with rms roughness ≈2.52 nm (b) at surface pressure 20mN/m, with rms roughness ≈3.19 nm, (c) the partial curve nature of spermine shown below AFM image.

The molecules follow expanded (E) to condensed (C) phase transition (E-C transition) at 293 cm^2 and linear to overturn U-shape transition (L-OU transition) after 192 cm^2. We presume that the molecules maintain their linear conformation at low surface pressure and as the pressure increases the plateau region starts building up and collapses at192 cm^2 which may correspond to the area of the molecule for fully bent conformation of the spermine with a lift off area of approximately to 12 $Å^2$ as compared to the linear confirmation at 293 cm^2 with a lift off area of 24 $Å^2$. As the surface area decreases below 192 cm^2, no more change in surface pressure was observed and we can infer that at this position the hydrophilic ends of spermine molecules should be anchored to the water subphase and this might result in partial protonation of the amine in spermine molecule leading to slight curve in a structure (hydrogen bonding between water and spermine) as shown below in **Fig. 3(c)**. Formation of structures are comparable to bolaamphiphile,1,12-dodecane diammonium ($C_{12}DA^{2+}$) which exhibited U-shaped confirmation in the presence of cucurbit [**5**] uril [**40**].

We further investigated the spermine monolayer (alone) by atomic force microscopy (AFM) to find out its bending behavior by observing the change in the roughness with the increase of surface pressure. **Fig. 3** (**a** and **b**) shows AFM images of the spermine monolayer for (sample A) at pressure 3mN/m and sample B at 20mN/m respectively. The height difference from the bottom to top of the image for (sample A) is 6 nM, and that for (Sample B) is 11 nM respectively. The surface roughness determined by AFM for the monolayer deposited on a silicon wafer substrate was averaged at three different points with the change of surface pressure approximately 2.52 and 3.19 nM respectively for both the samples and we can conclude that the surface roughness becomes more as the surface pressure increases from 3 to 20 mN/m. At low surface pressure, the spermine monolayer has a small surface roughness because the molecules might have a low height regardless of their structures. With the increase of surface pressure, the spermine molecules have different compression types according to the initial conformations of the carbon chains, which result in a large surface roughness of the monolayer [**32, 41**]. We can say that at greater surface pressure, the long carbon chain converts from a trans or gauche conformation, which occupies a smaller molecular area.

The hysteresis measurements (inset **Fig. 2(b)**) confirmed that these processes were reversible. However the monotonic decrease in surface area during compression at 192cm^2 is probably due to the existence of two secondary amines N-H at C6-C7/C6´-C7´[42-43]which allows the bending of molecule in U-shape at C6-C7/C6´-C7´carbon resulting in a condensed phase. This observation is quite contrary in the case of monoamines octadecylamine (ODA) **Fig. 2**(**a**) which shows a steep rising up to collapse pressure reached at about 16 mN/m [**44-45**]. The compressibility of the monolayer films can also be calculated according to the relation Equation1; where a_1 and a_2 are the areas per molecules at surface pressures π_1 and π_2 respectively [**46**].

$$C = -\frac{1}{a_1}\frac{a_2 - a_1}{\pi_2 - \pi_1} \tag{1}$$

It can be observed from the graphical representation that the compressibility of diamine monolayer is much more than the mono amine which shows a steep rise. It can be further seen from **Fig. 2(b)** that after approximately 3 hrs of spreading of spermine at the interface (curve 2 and 3), there is a left shift in the takeoff area (E to C transition point) which may be due to the fact that initially spermine molecule is soluble in the aqueous phase and it finally stabilizes after approx 3 hrs of spreading. This is also evident from the overlapping of the π-A isotherm (curve 3 and 4). They correspond to curves taken after 3 and 4 hrs of the spreading of the monolayer.

After observing the behavior of the diamaine on the aqueous subphase, π-A isotherm of spermine monolayer spread over the Au NPs colloidal subphase was examined. **Fig. 4** shows the schematic representation of the experimental setup for the expected behavior of gold nanoparticles in presence of diamine and proposed assembly.

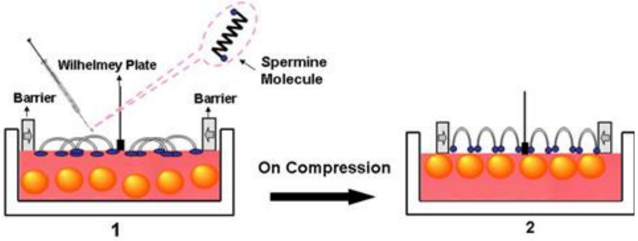

Fig. 4. Schematic illustration of spermine monolayer on AuNPs molecule on LB trough.

It was found that in the presence of Au NPs (**Fig. 5**, curve 1), the position of isotherm was majorly dependent on the time period given to spermine monolayer to bind to Au colloid subphase before compression. After a waiting time of 30 min, the isotherm exhibits a right shift and it clearly starts with higher lift-off area or we can say a more expanded (E) state in comparison to the pure spermine monolayer (Curve1, **Fig. 2(b)**), ascribable to the adsorption of Au NPs. While the adsorption time allotted to Au NPs was raised to 2.0 or 3.0 h, the π-A isotherm was found to shift left (**Fig. 5**)as compared to the waiting time of 30 min (Curve 1).

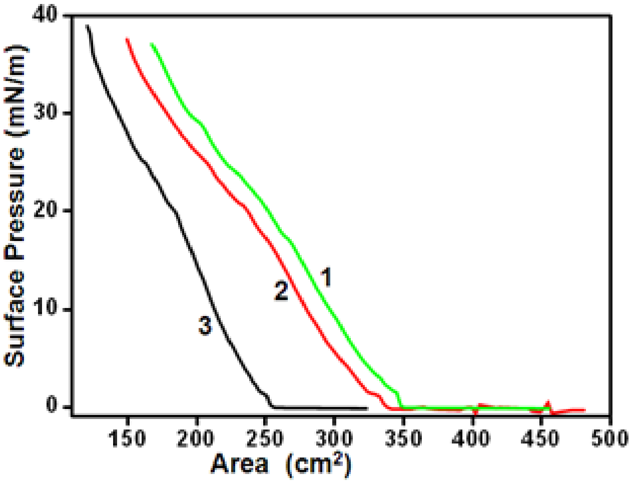

Fig. 5. Pressure-Area Isotherm of spermine monolayer on gold nano-particulates surface. Curve 1: after 30 min; Curve 2: after 2 h; Curve 3: after 3 h of spreading of monolayer.

This behavior might be due to the ability of the spermine monolayer to make contact with negatively charged AuNPs resulting in an increased electrostatic interaction. When a sufficient amount of spermine molecules bind to the AuNPs, the nanoparticle becomes more hydrophobic by contact angle measurements (not shown),and it becomes possible for the particle to exist at the interface rather than in the colloid phase as shown schematically in the sequence presented in **Fig. 6**. This is comparable to the observation in which DNA molecule entangle themselves in a random coil on reacting with spermine [**47**]. The fact that the spermine molecules have a fair degree of solubility in water is evident from the left shift in the isotherm as shown in **Fig. 5**, curve 2 and 3 indicating a decrease in area per molecule as the time frame increases.

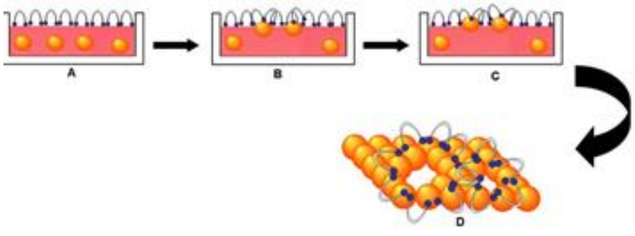

Fig. 6. Schematic illustrating the arrangement of gold NPs at different time intervals (A-C) and subsequent formation of the network (D) at the air-water interface.

It is to be mentioned here that the gold colloidal solution in the subphase was ruby red colored before spreading of spermine. However, after 10 min of spreading the spermine molecule at the interface, the colour of the subphase near the interface changed to purple colour on binding of AuNPs with diammine. This is similar to the observation for non-covalent bonding of AuNPs with amino groups in antibiotics [**48**]. This purple monolayer was stable, virtually unchanged for days, even with the barrier at the open position.

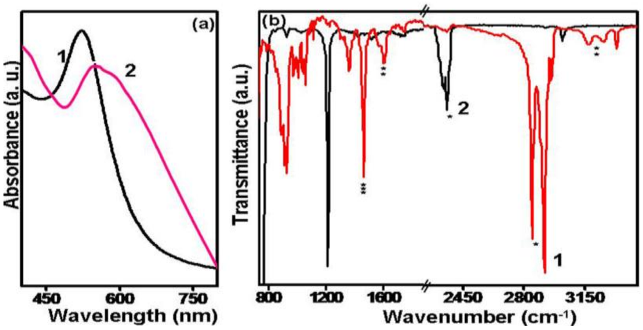

Fig. 7. (a) UV-vis spectra of colloidal gold nanoparticulates (curve 1); Film of gold NPs on quartz after complexation with spermine (curve 2) (b) FTIR spectra of pure spermine (curve 1, red colored) and gold film after capping of gold NPs with spermine at the air–water interface (curve 2, black colored) (**.**) dots indicate the important frequencies).

UV-Vis absorption spectrum of the spermine-AuNPs film showed an absorption band at 590 nm **Fig. 7(a)** (curve 2) with a considerable red-shift as compared to the absorption peak at 520 nm (curve 1) for as synthesized gold NPs. Red-shifts in the absorption wavelength have been observed in the past also [**49**], which is due to the plasmon coupling of gold NPs when in proximity, indicating assembly of the nanoparticles.

FT-IR studies confirmed the electrostatic interactions between spermine and gold indicating towards the possibility of spermine as an effective capping agent over gold NPs. **Fig. 7b** showed the FTIR peaks in the range of 800 - 3500 cm^{-1} for pure spermine (curve 1, red colored) and (curve 2, black colored) for spermine-gold NPs. The peaks at 3350 cm^{-1} and 1610 cm^{-1} (curve 1 , red colored) for spermine only clearly indicates the presence of N-H group due to the stretching and bending modes respectively whereas disappearance of peak at 3350 cm^{-1} (curve 2, black colored) can be attributed to the binding of spermine molecules with gold NPs at the two amine (-NH$_2$) ends. Moreover there is a slight shift in the methylene asymmetric and symmetric vibration modes at 2420 cm^{-1}indicated by a sharp peak in the case of spermine-gold NPs which confirms the capping of gold NPs with spermine [**50-51**].

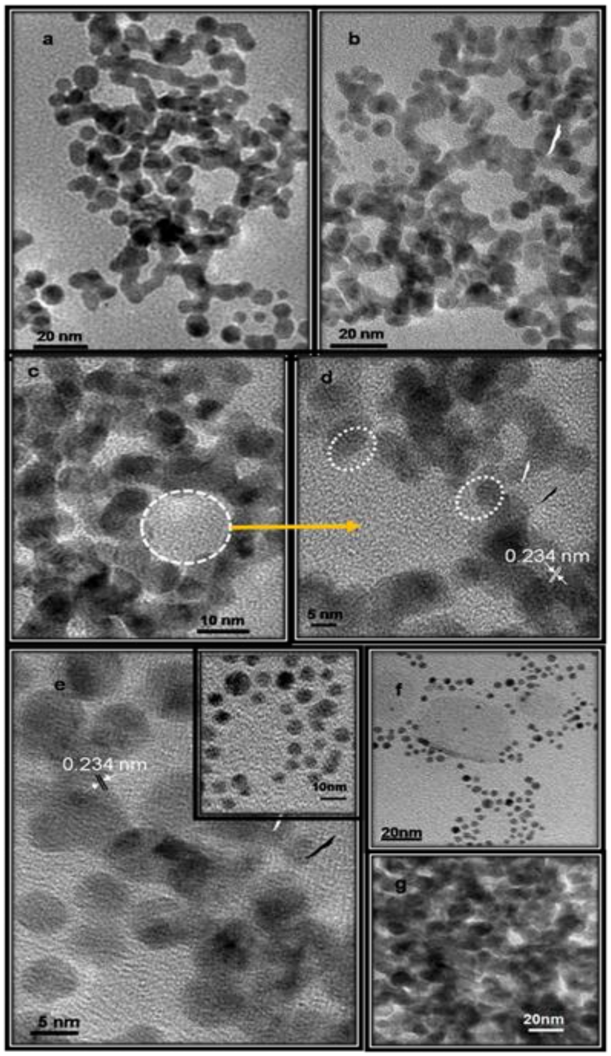

Fig. 8. Representative TEM images of spermine-gold nanostructures at low and high magnifications.(a,b): After 30 min of complexation. (c-d): higher magnification images of the interlinked gold nanostructures; outlined particles marked with circle show rings. (e,f) : After 10 min of complexation of spermine with gold nanoparticulates, Inset showing a lower magnification image (g): Multilayers showing interlinking networks formed after prolonged duration for interlinking.

To examine the adsorption behavior of spermine on AuNPs subphase and to explore the reasons for the left shift in the take off area, microscopy images of the Au-spermine monolayers were studied. Surface pressure was recorded using a Wilhelmy arrangement. Each isotherm was repeated and consistent results were obtained. The monolayers were deposited upstroke (lifting speed 5 mm min^{-1}) on carbon-coated copper TEM grids at a constant pressure of 30 mN/musing LB method of dip coating. The images obtained at different magnifications show a well pronounced three-dimensional spermine-AuNPs network. Detailed examination of the micrographs shown in **Fig. 8a** displays a low density of AuNPs for 30 min of adsorption time.

The density of nanoparticles in the film increased slightly when the adsorption time prolonged. However after waiting period of 3hrs, density of AuNPs remained almost the same but the interlinking of spermine-AuNPs networks increases indicating that this is the optimum time for particle adsorption to reach equilibrium state. During the interaction of spermine monolayer with Au-NPs, spermine adopts a curved or a bent confirmation that subsequently forms a ring like structures with AuNPs , this is quite similar to the observation found by Keniry and group, the bent structures of spermine were investigated by NMR studies [**42**]. Analogously Keniry had shown that spermine forms a non-linear confirmation (curved and gauche) with DNA quadruplexes that was further confirmed by molecular modeling studies [**43**]. It is to be noted that the networks when drop casted, at higher magnification, individual interlinked nanoparticles participate in the formation of ring like nanostructures that can be clearly distinguished as shown in the **Fig.8**(**a - f**) predictably due to diamine linkage.

The TEM micrographs also reveal average size of 10 nm for the interlinked nanoparticles, the narrow particle size distribution (**Fig. 8d**)and that the interlinked U-shaped nanoparticles form a loop or ring like structures wherein the loop structures per cluster increases with time.

Conclusion

The interlinked assemblies of gold NPs with spermine forms interlinked networks. π-Aisotherm clearly demonstrate the conformational change from linear to overturn U-shape for the spermine molecule on the Au-NPs subphase. The two hydrophilic ends (N-H) of the diamine anchored the gold colloidal surface while imparting the hydrophobic chains to rise up in the air generating an overturn U-shape. The assembly of the gold NPs with diamine provides more structural strictness and firmness to the amine-gold nanoparticle system resulting in the formation of networked loops. The dense film obtained with interesting morphology is a step towards modulating the assembly of the nanoparticles for bio-diagonostic property which is currently underway.

Acknowledgements

We would like to acknowledge the support and guidance of director NPL. Divya Sachdev thank Department of Science and Technology under project (DST SB/FT/CS-011/2013), Veeresh Kumar thank the Council of Scientific Industrial Research (CSIR) Govt. of India for the research fellowship and Shweta thanks DST (GAP 071232), Government of India for a research fellowship.

Reference

1. Kästle, G.; Boyen, H. G.; Weigl, F.; Lengl, G.; Herzog, T.; Ziemann, P.; Riethmüller, S.; Mayer, O.; Hartmann, C.; Spatz, J. P. *Adv. Funct. Mater.* **2003**, *13*, 853-861.
2. Rosi, N. L.; Mirkin, C. A. *Chem. Rev.* **2005**, *105*, 1547-1562.
3. Stokes, R. J.; Macaskill, A.; Lundahl, P. J.; Smith, W. E.; Faulds, K.; Graham, D. *Small* **2007**, *3*, 1593-1601.
4. Wang, Z. L. *Adv. Mater.* **1998**, *10*, 13-30.
5. Bandyopadhyay, K.; Patil, V.; Vijayamohanan, K.; Sastry, M. *Langmuir* **1997**, *13*, 5244-5248.
6. Colvin, V.; Goldstein, A.; Alivisatos, A. *J. Am. Chem. Soc.* **1992**, *114*, 5221-5230.
7. Freeman, R. G.; Grabar, K. C.; Allison, K. J.; Bright, R. M.; Davis, J. A.; Guthrie, A. P.; Hommer, M. B.; Jackson, M. A.; Smith, P. C.; Walter, D. G. *Science* **1995**, *267*, 1629-1632.
8. Mulvaney, P.; Giersig, M.; Henglein, A. *J. Phys. Chem.* **1993**, *97*, 7061-7064.
9. Niemeyer, C. M.; Bürger, W.; Peplies, J. *Angew. Chem. Int. Ed.* **1998**, *37*, 2265-2268.
10. Sastry, M.; Kumar, A.; Datar, S.; Dharmadhikari, C.; Ganesh, K. N. *Appl. Phys. Lett.* **2001**, *78*, 2943-2945.
11. Sastry, M.; Rao, M.; Ganesh, K. N. *Acc. Chem. Res.* **2002**, *35*, 847-855.
12. Kim, C.; Agasti, S. S.; Zhu, Z.; Isaacs, L.; Rotello, V. M. *Nature chemistry* **2010**, *2*, 962-966.
13. Kumar, A.; Ma, H.; Zhang, X.; Huang, K.; Jin, S.; Liu, J.; Wei, T.; Cao, W.; Zou, G.; Liang, X.-J. *Biomaterials* **2012**, *33*, 1180-1189.
14. Srivastava, S.; Kotov, N. A. *Soft Matter* **2009**, *5*, 1146-1156.
15. Kim, K.; Selvapalam, N.; Ko, Y. H.; Park, K. M.; Kim, D.; Kim, J. *Chem. Soc. Rev.* **2007**, *36*, 267-279.
16. Chernichko, D.; Khomutov, G. *Inorg. Mater.* **2009**, *45*, 1283-1288.
17. Khomutov, G.; Kislov, V.; Antipina, M.; Gainutdinov, R.; Gubin, S.; Obydenov, A. Y.; Pavlov, S.; Rakhnyanskaya, A.; Sergeev-Cherenkov, A.; Soldatov, E. *Microelectron. Eng.* **2003**, *69*, 373-383.
18. Khomutov, G. *Biophysics* **2011**, *56*, 843-857.
19. Giersig, M.; Khomutov, G. B. *Nanomaterials for application in medicine and biology*; Springer, 2008.
20. Ruiz-Hitzky, E.; Ariga, K.; Lvov, Y. M. *Bio-inorganic hybrid nanomaterials*; Wiley. com, 2008.
21. Brust, M.; Stuhr-Hansen, N.; Nørgaard, K.; Christensen, J. B.; Nielsen, L. K.; Bjørnholm, T. *Nano Lett.* **2001**, *1*, 189-191.
22. Damle, C.; Gole, A.; Sastry, M. *J. Mater. Chem.* **2000**, *10*, 1389-1393.
23. Heath, J. R.; Knobler, C. M.; Leff, D. V. *J. Phys. Chem. B* **1997**, *101*, 189-197.
24. Kotov, N.; Meldrum, F.; Wu, C.; Fendler, J. *J. Phys. Chem.* **1994**, *98*, 2735-2738.
25. Meldrum, F.; Kotov, N.; Fendler, J. *Langmuir* **1994**, *10*, 2035-2040.
26. Nakaya, T.; Li, Y.-J.; Shibata, K. *J. Mater. Chem.* **1996**, *6*, 691-697.
27. Mayya, K.; Patil, V.; Sastry, M. *Langmuir* **1997**, *13*, 2575-2577.
28. Mayya, K.; Sastry, M. *Langmuir* **1998**, *14*, 6344-6346.
29. Sastry, M.; Mayya, K.; Patil, V.; Paranjape, D.; Hegde, S. *J. Phys. Chem. B* **1997**, *101*, 4954-4958.
30. Spatz, J. P.; Mössmer, S.; Hartmann, C.; Möller, M.; Herzog, T.; Krieger, M.; Boyen, H.-G.; Ziemann, P.; Kabius, B. *Langmuir* **2000**, *16*, 407-415.
31. Fuhrhop, J. H.; Fritsch, D. *Acc. Chem. Res.* **1986**, *19*, 130-137.
32. Lee, J.; Joo, H.; Youm, S. G.; Song, S.-H.; Jung, S.; Sohn, D. *Langmuir* **2003**, *19*, 4652-4657.
33. Meguro, K.; Ikeda, K.; Otsuji, A.; Taya, M.; Yasuda, M.; Esumi, K. *J. Colloid Interface Sci.* **1987**, *118*, 372-378.
34. Menger, F.; Wrenn, S. *J. Phys. Chem.* **1974**, *78*, 1387-1390.
35. Rosen, M. J.; Baum, M.; Kasher, F. *J. Am. Oil Chem. Soc.* **1976**, *53*, 742-745.
36. Liquori, A.; Costantino, L.; Crescenzi, V.; Elia, V.; Giglio, E.; Puliti, R.; De Santis Savino, M.; Vitagliano, V. *J. Mol. Biol.* **1967**, *24*, 113-122.
37. Rasing, T.; Shen, Y.; Kim, M.; Grubb, S. *Phys. Rev. Lett.* **1985**, *55*, 2903.
38. Paczesny, J.; Wojcik, M. M.; Sozański, K.; Nikiforov, K.; Tschierske, C.; Lehmann, A.; Gorecka, E.; Mieczkowski, J.; Holyst, R. *Journal of Physical Chemistry C* **2013**, *117*, 24056-24063.
39. Vigderman, L.; Zubarev, E. R. *Advanced Drug Delivery Reviews* **2012**.
40. Baek, K.; Kim, Y.; Kim, H.; Yoon, M.; Hwang, I.; Ko, Y. H.; Kim, K. *Chem. Commun.* **2010**, *46*, 4091-4093.
41. Khomutov, G.; Antipina, M.; Gainutdinov, R.; Kislov, V.; Rakhnyanskaya, A.; Sergeev-Cherenkov, A.; Tolstikhina, A.; Yurova, T. *Materials Science and Engineering: C* **2003**, *23*, 903-908.

42. Keniry, M. A.; Owen, E. A. *FEBS Lett.* **2014**, *588*, 1949-1954.
43. Keniry, M. A.; Owen, E. *J.Mol.Recog.* **2013**, *26*, 308-317.
44. Lee, Y.-L. *Langmuir* **1999**, *15*, 1796-1801.
45. Petty, M. C. *Langmuir-Blodgett films: an introduction*; Cambridge University Press, 1996.
46. Gaines, G. L. *Insoluble monolayers at liquid-gas interfaces*; John Wiley & Sons, New York, 1966.
47. Kobayashi, K.; Tateishi-Karimata, H.; Tsutsui, K.; Wada, Y.; Sugimoto, N. *Chem. Lett.* **2011**, *40*, 855-857.
48. Burygin, G.; Khlebtsov, B.; Shantrokha, A.; Dykman, L.; Bogatyrev, V.; Khlebtsov, N. *Nano.Res.Lett.* **2009**, *4*, 794-801.
49. Patil, V.; Malvankar, R.; Sastry, M. *Langmuir* **1999**, *15*, 8197-8206.
50. Chandrasekharan, N.; Kamat, P. V. *Nano Lett.* **2001**, *1*, 67-70.
51. Teranishi, T.; Hosoe, M.; Tanaka, T.; Miyake, M. *J. Phys. Chem. B* **1999**, *103*, 3818-3827.

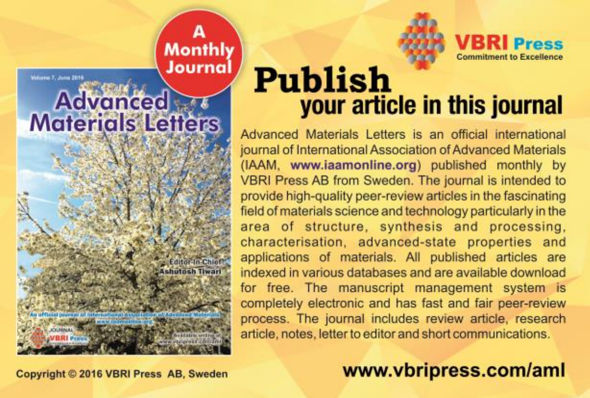

Supplementary Information

Studies performed on surfactant spermine CMC and critical angle

Spermine when dissolved in water significantly changes the its surface properties, particularly, surface tension. There is a decrease in the tension onincreasing the solubility and these changes do not occur until a minimum bulk surfactant concentration is reached i.e. critical micelle concentration (CMC).

Fig. S1 shows the CMC plot for spermine molecule. It can be seen from the graph that the arrangement of spermine molecule at the air water interface depends on the concentration of the amphiphiles, with the increase in spermine concentration, the arrangement shifts to formation of micelles. This concentration above which the micelles form with increase in number of spermine molecules is called the Critical Micelle Concentration (CMC). Surface tension technique was used to measure CMC.

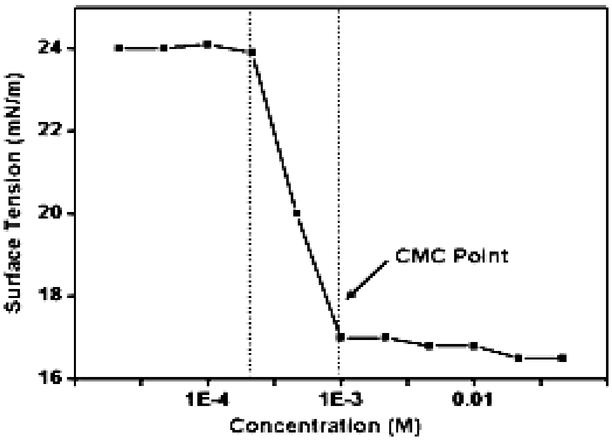

Fig. S1. Critical Micelle Concentration of spermine.

Fig. S1 we observe three phases:

1. At very low concentrations of the surfactant, only slight change in surface tension is detected.
2. Additional surfactant decreases the surface tension.
3. When the surface becomes fully loaded, no further change in surface tension is observed.

As shown above, the technique for assaying CMC by measurement of surface tension is simple and straightforward. A graph of the surface tension versus log concentration is produced. The CMC is found as the point at which the two lines intersect; the baseline of minimal surface tension and the slope where the surface tension shows linear decline. Therefore CMC for spermine is 10^{-3} M. The orientation and arrangement of molecules on the LB films are affected by the surface pressure and transferring rate.

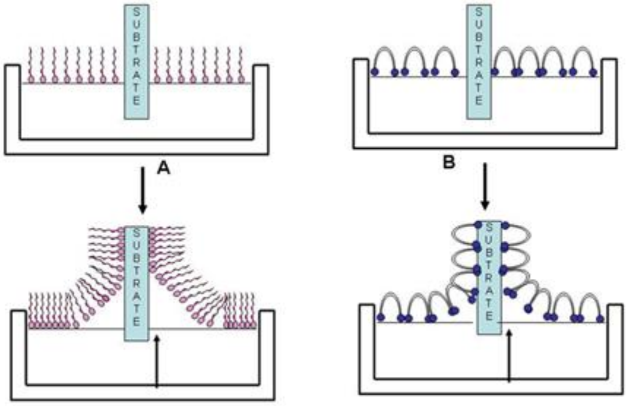

Fig. S2. Schematic illustration showing the variation in arrangement of monoamine and diamines on substrate.

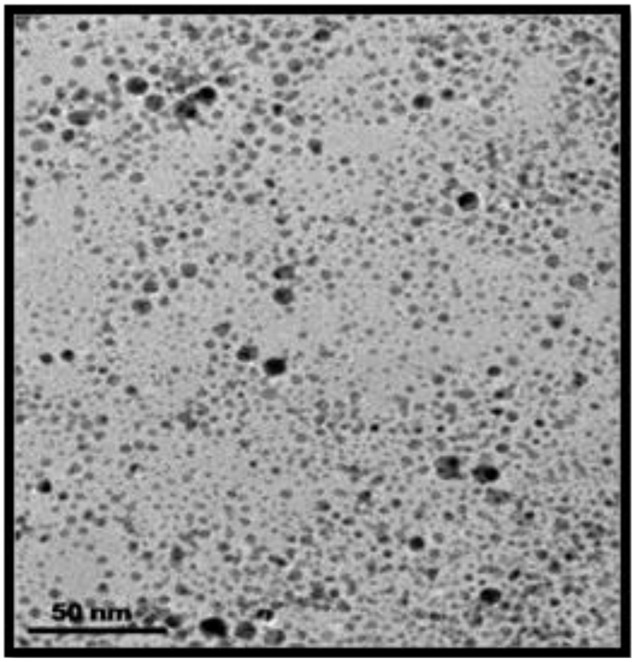

Fig. S3. Micrograph of grid with drop casted solution of citrate stabilized-AuNPs.